Two-Dimensional Numerical Study of Cross-Flow Filtration Combustion

Transition metal nitrides can be synthesized in the combustion regime using a self-propagating, high-temperature synthesis by the process of filtration combustion. A detailed two-dimensional numerical study for the filtration combustion process in the cross-flow configuration is presented. The process is modeled by a two-dimensional pseudohomogenous model. The model equations, which are very stiff and exhibit varying time and length scales, are solved using finite differences on a two-dimensional orthogonal adaptive mesh. The effects of pressure, bed height and bed porosity on combustion front propagation and final conversion are studied. A series of full simulations for the titanium-nitrogen system shows good agreement between theoretical predictions and experimental observations.

Hemant W. Dandekar
Jan A. Puszynski
Vladimir Hlavacek
Laboratory of Ceramic and
Reaction Engineering
Department of Chemical Engineering
State University of New York at Buffalo
Amherst, NY 14260

Introduction

Transition metal nitrides are usually synthesized on a commercial scale by direct reaction of metal with nitrogen under almost isothermal conditions. This process often takes several hours, and the product quality is often affected adversely by incomplete conversion of solid reactant. Furthermore, additional production cycles are required to completely convert the partially converted reactant in a high-temperature furnace. Since the direct reactions of transition metals with hydrogen and nitrogen are characterized by high activation energy and heat of reaction, it is possible to ignite fine metallic powders and to maintain a self-sustaining process. The reactions, however, occur in the combustion regime; therefore, the dynamics of these systems are complex and it is very difficult to predict *a priori* without detailed numerical modeling. Numerical modeling also helps better understand the heat and mass transfer characteristics of the system.

The goal of this study is to analyze the combustion process between metal powder and gaseous oxidizer in two dimensions. The process is referred to as filtration combustion, which has been studied in the past by other authors (Merzhanov et al., 1973, 1975). Early pioneering studies in filtration combustion can be found in Russian literature of the 70's, mostly by Aldushin and coworkers (1974, 1976, 1980). Most of these studies were analytical in nature and helped define the basic regimes for combustion synthesis and establish the importance of parameters like pressure, thermal conductivity and permeability, and their effect on front propagation and final conversion of the product.

In the early 80's, stability analyses for filtration combustion systems were presented by Sukhov and Yarin (1980) and Aldushin and Kasparayan (1981). While the latter study was detailed, and considered different kinds of flow configurations and factors leading to two-dimensional instabilities like nonplanar combustion front propagation, there were no numerical calculations for two-dimensional models to confirm the predictions made from simplified analytical models.

Munir and Holt (1987) have performed a theoretical analysis for formation of refractory metal nitrides under conditions when sufficient gas is present in the system for the combustion to take place in the kinetic regime. On the basis of thermodynamic and kinetic considerations they have derived certain minimum values of pressures required for nitridation. A recent experimental study (Agrafiotis et al., 1990) has shown that the actual pressure required for nitridation for certain systems is much lower than that predicted by Munir and Holt.

Munir (1988), in a recent publication, has given a thorough review of the various products that can be obtained by combustion synthesis. Again the importance of operating pressure has been stressed.

Degreve et al. (1987) have presented calculations for 1-D and 2-D filtration combustion cases to illustrate the use of adaptive meshes in simulation of combustion front phenomena. Calculations for countercurrent filtration in two space dimensions have been presented for the first time. Presence of oscillating fronts

and corrugated nonplanar fronts with moving hot spots were predicted for systems with very high activation energies and extreme exothermicity.

Dandekar et al. (1990) have presented a detailed study of countercurrent filtration combustion, for adiabatic and nonadiabatic systems. This configuration is shown in Figure 1. It has been shown that at high pressures stability criteria for solid-solid systems can be extended to gas-solid systems. At very low pressures all systems always propagate with constant front velocity.

There are, however, certain limitations of the counterflow configuration, which make it unsuitable for industrial-scale production. The length of the reactor is limited as it controls the length of the filtration path. Hence, high pressures are required to maintain a reasonable pressure gradient to drive the flow of gaseous reactant. At low pressures, pore closures due to volumetric expansion/sintering will prevent conversion of the inner layers of the solid. Furthermore, in the case where the product is a fused solid, its removal from a closed cylindrical reactor is another problem. Taking these drawbacks into account, a new configuration, called the cross-flow configuration, is proposed, Figure 2. Gas accessibility to the combustion front is significantly improved in the cross-flow configuration. Gaseous reactant is transported from surroundings not only by longitudinal flow from above, but also by transverse (countercurrent) flow from regions ahead of the front. As a result, the nitridation reaction can be completed at lower pressures compared to the countercurrent configuration. Furthermore, the configuration uses a reactor open at the top, which facilitates product removal. This configuration was first proposed by Kumar et al. (1988).

A wealth of information is available for the counterflow configuration; however, there is no information for two-dimensional reaction front patterns for the cross-flow configuration. This study aims at simulating a two-dimensional model for

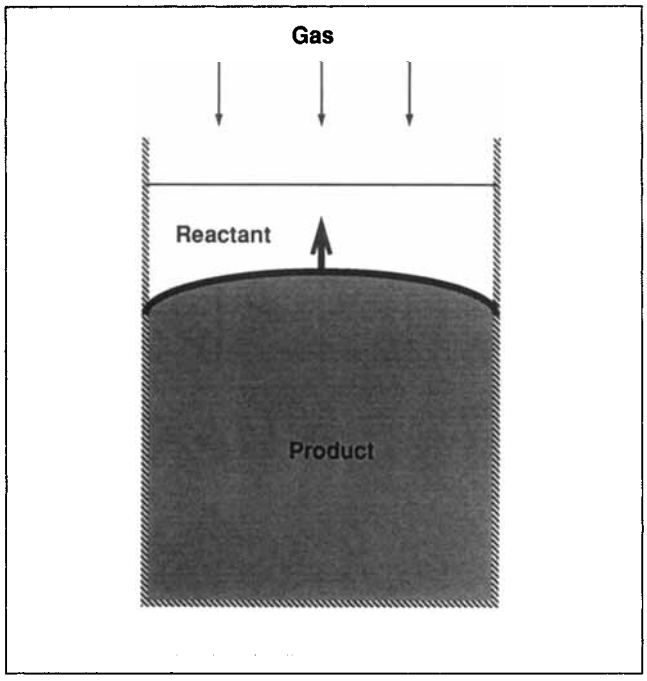

Figure 1. Counterflow filtration combustion configuration.

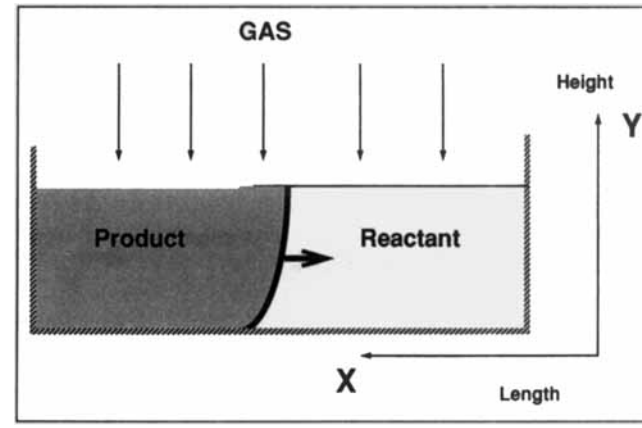

Figure 2. Cross-flow filtration combustion configuration.

the cross-flow configuration, which we hope offers an understanding of the basic engineering aspects, specifically:

- What conditions are necessary for complete conversion and what front propagation phenomena can exist?
- Since there are no real limitations on the length scales in the direction of reaction front propagation, it is very important to explore the maximum bed height to achieve complete conversion, especially at low pressures.
- Study the effect of bed porosity on front propagation and consequently final conversion. Porosity changes can occur due to volumetric expansion of the bed during synthesis which might curtail the access of gas to the inner layer.
- Finally compare qualitatively numerical results with experimental observations to verify the model.

Model Formulation

The model equations formulated here describe the filtration combustion process under cross-flow configuration. The reactor, which is in the form of a flat-bottomed rectangular container filled with metallic powder, is kept under an atmosphere of nitrogen under suitable pressure. The reaction is initiated by a short-term energy source such as a resistively heated graphite or tungsten strip. Once ignited, the reaction continues on its own in the form of a steep reaction front which separates unreacted solid from the products. The front propagates down the length of the boat while the gas is drawn in perpendicular to the direction of front propagation. The flow is driven by the pressure gradient imposed by the consumption of nitrogen at the front and the pressure outside. Inside the system, the reaction occurring between the pure gaseous oxidizer G and the particles of solid reactant S results in a solid product P according to:

$$R(s) + \mu G(g) \rightarrow (1 + \mu)P(s) \qquad (1)$$

where 1 kg solid + μ kg gaseous oxidizer $\rightarrow$ $(1 + \mu)$ kg solid product.

The reaction between solid and gas inside the system occurs at the particle level. Hence, one must use a suitable model to find a relation beween reaction kinetics at the particle level and the reaction rate per unit volume of the bed. At the particle level, the intrinsic reaction rate or the diffusion throughout the product layer may be the controlling factors governing the particle level kinetics. Depending on the controlling factors, dependence of

the reaction rate on the particle size varies. For systems like $Ta - N_2$, the rate is independent of particle size, where the porous particles react at the same rate as the nonporous particles. This can be explained using the 'grain model' (Szekly et al., 1972). For the case of $Ti - N_2$ the reaction rate is inversely proportional to the the square of the particle size (Agrafiotis, 1990), suggesting a diffusional mechanism controlling the reaction rate. Thus, the model can be reduced to a phenomenological expression of the form:

$$r_s = \rho_s^o k_o f(\eta) \exp(-E/RT) p^\nu \tag{2}$$

where k_o is the preexponential factor which is a function of the average particle size of the solid reactant among others. The dependence of the overall rate on fractional conversion η can appear in several possible forms. The function $f(\eta)$ can be represented as $f(\eta) = (1 - \eta)^n$, where n can vary from $\frac{1}{3}$ to $\frac{2}{3}$ depending on the controlling mechanism in the shrinking core model. Usually the reaction is a much stronger function of the temperature than the particle conversion, given the high activation energies of the reactions. While a more refined expression can be obtained using the shrinking core model for spherical particles, a simplified form $f(\eta) = (1 - \eta)$ is used, which is the upper limit of the reaction rate dependence on fractional conversion.

Before writing down governing equations, several additional assumptions have been made to make the model equations describing the filtration combustion process suitable for numerical simulations.

- The system comprised solid powder and gaseous oxidizer is considered to be pseudohomogeneous. This implies that the temperature of the solid particles and their surrounding area is taken to be identical, and the heat balance can be taken over by the whole system, instead of over solid and gas separately, especially if it is assumed that reaction-diffusion processes inside the solid particle respond very fast to the changing surrounding conditions. Thus any change in parameters like density of gas or temperature in the bulk phase is felt instantly at the surface of the particle and *vice versa*. The heat transfer resistance between the particle and the bulk can be neglected given the high pressures of operation which lead to high film heat transfer coefficients. Then the overall phenomenological reaction rate expression can be inserted into governing equations directly.
- The physical properties of the individual solid components (specific heat, density, and thermal conductivity) and gas (specific heat and thermal conductivity) are assumed constant.
- The thermal conductivity of the porous bed is taken as a linear function of the bed porosity. While in reality the effective thermal conductivity of the bed is a function of the gas flow rate through the bed, the temperature and pressure of operation, variation with respect to the bed porosity was the only factor taken into account to keep the numerical calculations more manageable.

$$\lambda = (1 - \epsilon)\lambda_s + \epsilon\lambda_g \tag{3}$$

- The heat conduction process in the system can be described by Fourier's law.
- Pressure effects of the gas phase are neglected in the energy balance.
- Porosity changes due only to volumetric expansion of the reactants to form products have been taken into account. Melting or sintering has not been considered. Melting can be neglected for systems in which the solid reactant and product melt at temperatures much higher than the reaction temperature (e.g., $Ta - N_2$) or when the initial reaction mixture is diluted with the product. In this study, titanium has been diluted by at least 50% titanium nitride so that melting effects on porosity are not significant.
- The volumetric heat capacity of the pseudohomogeneous phase is taken as a linear function of porosity.

$$\rho \overline{C} = \epsilon\rho_g C_g + (1 - \epsilon)\rho_s C_s \tag{4}$$

- Permeability of the bed is a strong function of the porosity, and its dependence is given by the Kozeny Carman equation (Carman, 1938).
- The equation of state of the gaseous reactant is given by the ideal gas law.
- Gas flow through the porous permeable medium under the action of pressure gradients is governed by Darcy's law.
- No dissociation of the formed product occurs.

The filtration combustion system is described by the following nonlinear parabolic-hyperbolic partial differential equations.

Mass balance on the gas phase:

$$\frac{\partial \epsilon\rho_g}{\partial t} = -\frac{\partial(\epsilon\rho_g v_x)}{\partial x} - \frac{\partial(\epsilon\rho_g v_y)}{\partial y} - \mu W_s \tag{5}$$

Energy balance on the system:

$$\frac{\partial(\epsilon\rho_g c_g + (1 - \epsilon)\rho_s c_S)T}{\partial t} = \frac{\partial}{\partial x}\lambda\frac{\partial T}{\partial x} + \frac{\partial}{\partial y}\lambda\frac{\partial T}{\partial y} - \frac{\partial(\epsilon\rho_g v_x c_g T)}{\partial x} - \frac{\partial(\epsilon\rho_g v_y c_g T)}{\partial y} + (-\Delta H)W_s \tag{6}$$

(The derivation of this equation can be found in the Supplementary Material.)

Equation of state:

$$p = \frac{\rho_g RT}{M_g} \tag{7}$$

Darcy's law:

$$v_x = -k\frac{\partial p}{\partial x} \quad v_y = -k\frac{\partial p}{\partial y} \tag{8}$$

Reaction rate expression:

$$\frac{\partial \rho_R}{\partial t} = -W_s = -\rho_R^o k_o f(\eta) \exp(-E/RT) p^\nu \tag{9}$$

The term $(1 - \epsilon)\rho_s c_s$ represents the contribution of the solid heat capacity to the pseudohomogenous-phase heat capacity and can be expanded to:

$$(1 - \epsilon)\rho_s c_s = \rho_R c_R + \rho_P c_P \tag{10}$$

To render the equations dimensionless, the following scaling relations will be used for the independent and dependent variables

$$\bar{t} = t/t_* \quad \bar{\lambda} = \lambda/\lambda_s \tag{11}$$

$$\bar{x} = x/x_* \quad \bar{y} = y/x_* \tag{12}$$

$$x_*^2 = \frac{\lambda t_*}{\rho_R^o c_R} \quad t_* = \frac{E(-\Delta H)\exp(E/RT_*)}{RT_*^2 c_R k_o p^{o^r}} \tag{13}$$

$$\rho_P = \rho_R^o(1+\mu)\eta \quad \theta = \frac{E}{RT_*}\frac{(T-T_*)}{T_*} \tag{14}$$

$$\bar{\rho}_g = \rho_g/\rho_g^o \quad \pi = p/p^o \tag{15}$$

$$\bar{v}_x = v_x/v_* \quad \bar{v}_y = v_y/v_* \tag{16}$$

$$v_* = x_*/t_* \quad \bar{\epsilon} = \epsilon/\epsilon^o \tag{17}$$

$$\bar{h}_r = x_* h_r/\lambda_s \quad \bar{h}_c = x_* h_c/\lambda_s \tag{18}$$

The scaling used here for the reduction of the equations to dimensionless form is standard in the combustion literature (Merzhanov et al., 1973; Merzhanov and Borovinskaya, 1975). The scaling variable x_* represents an approximate measure of the heating zone length, and x_*/t_* is an approximate measure of the reaction front propagation velocity.

The variation of porosity due to the volumetric changes caused by the reaction is assessed using the density of solid reactant obtained from Eq. 9. This, combined with the expressions below, yields the porosity at any instant. Note that the ρ_R and ρ_P are *bulk* densities of the solid reactant.

$$\eta = 1 - \rho_R/\rho_R^o \tag{19}$$

$$\epsilon = \epsilon^o + (1-\epsilon^o)(1-Z)\eta \tag{20}$$

Substitution into the dimensional equations result in the following dimensionless equations governing the filtration combustion process.

Mass balance on the gas phase:

$$\frac{\partial \alpha\bar{\epsilon}\bar{\rho}_g}{\partial \bar{t}} = -\frac{\partial(\alpha\bar{\epsilon}\bar{\rho}_g\bar{v}_x)}{\partial \bar{x}} - \frac{\partial(\alpha\bar{\epsilon}\bar{\rho}_g\bar{v}_y)}{\partial \bar{y}} - \gamma^{-1}R \tag{21}$$

Heat balance on the system:

$$\frac{\partial(\alpha\delta_1\bar{\epsilon}\bar{\rho}_g + 1 - \eta + \delta_2\eta)\theta}{\partial \bar{t}} = \frac{\partial}{\partial \bar{x}}\bar{\lambda}\frac{\partial \theta}{\partial \bar{x}} + \frac{\partial}{\partial \bar{y}}\bar{\lambda}\frac{\partial \theta}{\partial \bar{y}} - \frac{\partial(\alpha\delta_1\bar{\epsilon}\bar{\rho}_g\bar{v}_x\theta}{\partial \bar{x}} - \frac{\partial(\alpha\delta_1\bar{\epsilon}\bar{\rho}_g\bar{v}_y\theta)}{\partial \bar{y}} + [(1+\delta_1-\delta_2)(\beta\gamma)^{-1} + \gamma^{-2}]R \tag{22}$$

Equation of state:

$$\pi = \frac{\bar{\rho}_g(1+\beta\theta)}{(1+\beta\theta^o)} \tag{23}$$

Darcy's law:

$$\bar{v}_x = -\omega\frac{\partial \pi}{\partial \bar{x}} \quad \bar{v}_y = -\omega\frac{\partial \pi}{\partial \bar{y}} \tag{24}$$

Reaction rate expresson:

$$\frac{\partial \eta}{\partial \bar{t}} = \gamma^{-1}f(\eta)\exp\left(\frac{\theta}{1+\beta\theta)}\right)\pi^v = \gamma^{-1}R \tag{25}$$

A number of dimensionless parameters appear after dimensionalization. They are:

$$\alpha = \frac{\epsilon^o\rho_g^o}{\mu\rho_R^o} \quad \omega = \frac{kp^o\rho_R^o c_R}{\lambda_s} \tag{26}$$

$$\beta = \frac{RT_*}{E} \quad \gamma = \frac{c_R RT_*^2}{E(-\Delta H)} \tag{27}$$

$$\delta_1 = \frac{\mu c_g}{c_R} \quad \delta_2 = \frac{(1+\mu)c_P}{c_R} \tag{28}$$

The permeability dependence on porosity is given by the Kozeny-Carman equation, which in dimensionless form looks like:

$$\frac{\omega}{\omega_o} = \frac{\epsilon^3(1-\epsilon_o)^2}{\epsilon_o^3(1-\epsilon)^2} \tag{29}$$

To complete the formulation of the problem, initial and boundary conditions have to be specified on the system. In dimensionless form, they can be written as follows.

Initial conditions:

for $\bar{t} = 0$ and $0 \le \bar{x} \le L_x$, $0 \le \bar{y} \le L_y$

$$\theta = \theta^o \quad \eta = 0 \tag{30}$$

$$\bar{\rho}_g = 1 \quad \pi = 1 \tag{31}$$

$$\bar{v}_x = 0 \quad \bar{v}_y = 0 \tag{32}$$

Boundary conditions:

for $\bar{t}_H > \bar{t} > 0$ and $\bar{x} = L_x$, $0 \le \bar{y} \le L_y$

$$\theta = \theta^H \quad \bar{v}_x = 0 \tag{33}$$

for $\bar{t} > \bar{t}_H$ and $\bar{x} = L_x$, $0 \le \bar{y} \le L_y$

$$-\bar{\lambda}\frac{\partial \theta}{\partial \bar{x}} = \bar{h}_c(\theta - \theta^o) \quad \bar{v}_x = 0 \tag{34}$$

$\bar{y} = L_y$, $0 \le \bar{x} \le L_x$

$$-\bar{\lambda}\frac{\partial \theta}{\partial \bar{y}} = \alpha\delta_1\bar{v}_y[(\bar{\epsilon}\bar{\rho}_g\theta)^o - (\bar{\epsilon}\bar{\rho}_g\theta)] + \bar{h}_c(\theta - \theta^o) + \bar{h}_r(\theta - \theta^o) \quad \pi = 1 \tag{35}$$

$0 \le \bar{x} \le L_x, \bar{y} = 0$

$$-\bar{\lambda}\frac{\partial\theta}{\partial\bar{y}} = \bar{h}_c(\theta - \theta^o) \quad \bar{v}_y = 0 \tag{36}$$

$0 \le \bar{y} \le L_y, \bar{x} = 0$

$$-\bar{\lambda}\frac{\partial\theta}{\partial\bar{x}} = \bar{h}_c(\theta - \theta^o) \quad \bar{v}_x = 0 \tag{37}$$

The boundary conditions imply a nonadiabatic system with convective heat losses from all sides. Radiative heat losses are accounted for only at the top. The calculation procedure and numerical values used for the heat loss coefficients are available in Dandekar et al. (1990). Ignition by a thermal energy source takes place at $\bar{x} = L_x$, where the wall is also impermeable to gas penetration. The wall is heated to a temperature θ^H for a period of time t^H, which is of the order of a few seconds. The value of θ^H is typically the adiabatic temperature of the reaction. The side of the system at $\bar{y} = L_y$ is open to the outer atmosphere and the system can thus freely take up additional gaseous oxidizer under the right conditions.

Numerical Method

The two-dimensional model of the filtration combustion process represents a system of coupled, highly nonlinear, parabolic-hyperbolic, partial differential equations, exhibiting solutions with steep gradients which move rapidly over the space. Ideally, a good numerical method should have desirable features such as simplicity, accuracy, wide range of stability and efficient utilization of hardware. Realistically, trade-offs need to be made between these features to come up with a scheme best suitable for a particular application.

The main challenge lies in resolution of very high gradients in the space, which are confined to thin isolated regions. The use of equispaced grids for resolution of such gradients will require a phenomenally large number of points. Typically 10^3–10^4 grid points may be necessary. There are two ways to overcome these problems: adaptive grids and use of efficient time integration schemes.

While two-dimensional adaptive grids have been used in the past and codes are readily available, for the sake of simplicity (to avoid a control volume formulation), separate one-dimensional adaptation is performed in the X and Y direction. This keeps the mesh orthogonal, and simple finite differences on a nonequidistant mesh points can be applied. Details of the adaptive mesh are available elsewhere (Degreve, 1990). A moving mesh is used essentially, based on the distribution of a fixed number of points in regions of high gradients. This distribution is performed on the basis of weight functions, calculated taking into account the gradients and curvature of the temperature and concentration profiles. The weight functions are diffused so that the adaptive mesh need not be calculated at every time step. After every call to the adaptive mesh routine, the profiles are interpolated to the new mesh. The mesh is recalculated depending on the speed of propagation of the front, typically every five to ten time steps.

The first and second derivatives for a scalar entity ϕ are approximated by:

$$\frac{\partial\theta}{\partial y} = \frac{\phi_{i,j} - \phi_{i,j-1}}{y_j - y_{j-1}} \tag{38}$$

$$\frac{\partial^2\phi}{\partial y^2} = \frac{2}{y_{j+1} - y_{j-1}}\left[\frac{\phi_{i,j+1} - \phi_{i,j}}{y_{j+1} - y_j} - \frac{\phi_{i,j} - \phi_{i,j-1}}{y_j - y_{j-1}}\right] \tag{39}$$

All dependent variable values are defined on cell corners at grid points, while the velocities are defined between two grid points. Thus:

$$\bar{v}_x(i,j) = -\omega\left[\frac{\pi_{i,j} - \pi_{i-1,j}}{\bar{x}_{i,j} - \bar{x}_{i-1,j}}\right] \tag{40}$$

$$\bar{v}_y(i,j) = -\omega\left[\frac{\pi_{i,j} - \pi_{i,j-1}}{\bar{y}_{i,j} - \bar{y}_{i,j-1}}\right] \tag{41}$$

The donor cell method is used for convective terms (see Figure 3). This method is described by Roache (1972). The method possesses both the conservative and transportive properties, and retains something of the second-order accuracy of centered-space derivative. Therefore,

$$\frac{\partial v_x\phi}{\partial x} = \frac{\phi_R - \phi_L}{(\Delta\bar{x}_i + \Delta\bar{x}_{i-1})/2} \tag{42}$$

where

$$\phi_L = [(V_i + |V_i|)\phi_{i-1} + (V_i - |V_i|)\phi_i]/2$$

and

$$\phi_R = [(V_{i+1} + |V_{i+1}|)\phi_i + (V_{i+1} - |V_{i+1}|)\phi_{i+1}]/2$$

For relatively dense powder compacts, the permeability coefficient is low; as a result, the characteristic time for the system depends on the source term rather than the convection term. While an implicit scheme for time integration will provide stable solutions with a larger time step than an explicit time integration scheme, these time steps are not realized due to the limitations imposed by very small characteristic times attributed to the very fast reaction rates. Hence, an explicit scheme is used, which vectorizes completely.

The time step is controlled by stability considerations due to diffusion and convection. Thus, for a two-dimensional grid (Roache, 1972),

$$\frac{1}{(\Delta t)_{\max}} \ge \frac{|v_x|}{\Delta x} + \frac{|v_y|}{\Delta y} + 2\nu_s\left(\frac{1}{\Delta x^2} + \frac{1}{\Delta y^2}\right) \tag{43}$$

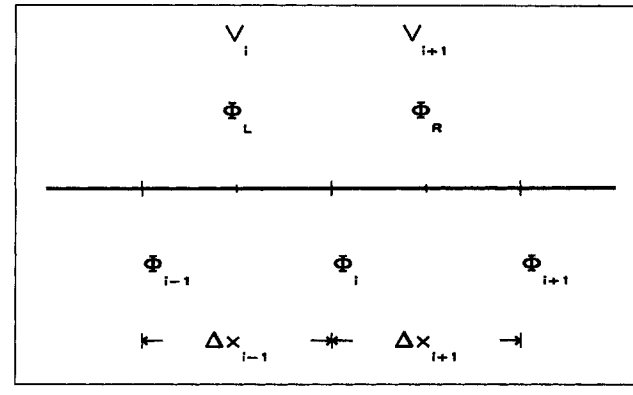

Figure 3. Donor-cell upwind differencing.

The diffusion term can be due to the thermal diffusivity or the *pseudodiffusivity of the pressure* due to calculation of velocity using Darcy's Law. Looking back at the density equation (minus the source term):

$$\alpha\epsilon \frac{\partial \overline{\rho}}{\partial t} = \alpha\epsilon \frac{\partial \overline{v}_x \rho}{\partial \overline{x}} + \alpha\epsilon \frac{\partial \overline{v}_y \rho}{\partial \overline{y}} \tag{44}$$

$$\overline{v}_x = -\omega \frac{\partial \pi}{\partial \overline{x}} \tag{45}$$

$$\overline{v}_y = -\omega \frac{\partial \pi}{\partial \overline{y}} \tag{46}$$

writing $\overline{\rho}$ as $\overline{\rho} = \pi(1 + \beta\theta_o)/(1 + \beta\theta)$ in Eq. 45 and assuming that the temperature essentially remains constant while gas flow takes place (for $\omega \gg 1$) we have

$$\frac{\partial \pi}{\partial t} = \frac{\partial}{\partial \overline{x}}\left(\pi\omega \frac{\partial \pi}{\partial \overline{x}}\right) + \frac{\partial}{\partial \overline{y}}\left(\pi\omega \frac{\partial \pi}{\partial \overline{y}}\right) \tag{47}$$

Using a maximum value of $\pi = \pi_o = 1$ in the righthand side, the following equation results:

$$\frac{\partial \pi}{\partial t} = \frac{\partial}{\partial \overline{x}}\left(\omega \frac{\partial \pi}{\partial \overline{x}}\right) + \frac{\partial}{\partial \overline{y}}\left(\omega \frac{\partial \pi}{\partial \overline{y}}\right) \tag{48}$$

Hence ω is the *pseudopressure diffusivity*.

Thus ν_s in the stability criterion is taken as the maximum value of ω and λ. Hence, the maximum allowable time step is calculated for each cell, and a minimum of these is taken for the entire domain. Using this procedure, one can automatically regulate the time step during the course of the calculation.

Most physical systems involving loose powders have a relatively large value of dimensionless permeability coefficient ($\omega \sim 100$) compared to the dimensionless thermal conductivity ($\lambda \sim 1$) at high pressures. Thus, the limiting factor is no longer the reaction rate term, but the convective term. To get around these severe limitations in time step, imposed by the high-*pseudopressure diffusivity* an alternative algorithm is used for high-permeability cases. In this algorithm, a fully implicit time integration scheme is used with quasilinearized reaction rate terms. The resulting system of linear equations is solved using successive overrelaxation. Typically two to three iterations are required at each step.

Significance of Parameters

The procedure of making the model equations dimensionless makes the numerical solution more tractable; however, this often leads to a loss of immediate realization of the physical significance of the large number of dimensionless parameters. Hence, it will be prudent to explain the physical significance of certain key dimensionless parameters before we discuss the results.

The parameters β and γ represent the dimensionless activation energy and heat of reaction. Low β or γ values represent a system with high activation energy or heat of reaction and *vice versa*. Parameter α represents the ratio of the amount of gas initially present inside the system to the amount of gas required to bring the reaction to full conversion. Thus, for $\alpha \simeq 1$ there is sufficient gas present in the pores to completely convert the solid reactant to a product. The value of α is directly related to the external pressure, and typical operating values are shown in Table 1 for nitrogen in the nitridation of transition metals. Thus α can be as low as 0.005 even at a relatively high pressure of 10 atm.

The system temperature is made dimensionless using the adiabatic temperature of the reaction as the reference value. Thus, the dimensionless temperature values are typically negative with the adiabatic temperature of the reaction being $\theta = 0$.

The parameter ω is the dimensionless permeability coefficient and signifies the ratio of width of the filtration zone to the heating zone. Thus, for high values of ω ($\omega \gg 1$) the gas flows at a much faster rate than the rate of front propagation and *vice versa*.

The parameters δ_1 and δ_2 give the ratio of specific heats of the gas and product to that of the solid reactant.

Table 1 gives the values of some of the physical properties corresponding to the dimensionless parameters used in this simulation.

The parameter Z is the ratio of volume of solid product at complete conversion ($\eta = 1$) to the volume of initial solid reactant. The solid expands if $Z > 1$ and contracts if $Z < 1$; thus causing a decrease or an increase in porosity, respectively. Some values for transition metal nitrides are shown in Table 2.

Results from Numerical Simulation

The simulation runs were performed on a CRAY X-MP/48 at the National Center for Supercomputing Applications at the University of Illinois at Urbana-Champaign. Typically 50–70 minutes of CPU time was required for each simulation, in spite of almost 90% vectorization of the DO loops in the program. An important question to be addressed was the visualization of the data produced from these simulations; typically each run would generate anywhere from 64,000 to 640,000 floating numbers depending on the number of profiles written.

The results are discussed in terms of the effects of pressure, bed height and porosity, and then compared with experimental values. Most of the data have been presented in the form of contour plots; however, some three-dimensional perspective plots are shown for high and low pressures including velocity vector plots to give the reader a feel for the flow patterns and the steep gradients which are encountered in these systems. Simulation results for the cases of high and low pressures were saved in the form of several hundred time profiles. Each of these profiles generated a single frame depicting the temperature or the concentration of the system. These frames were animated on a SUN Sparcstation 1 to study the nature of front propagation. Details of this method are available elsewhere (Dandekar, 1989).

Table 1. Physical Values Corresponding to Dimensionless Parameters

Parameter Range	Physical Value Range
$0.08 \le \beta \le 0.245$	$240 \ge E \ge 80$ kJ/mol
$0.03 \le \gamma \le 0.065$	$370 \ge (-\Delta H) \ge 170$ kJ/mol
$0.005 \le \alpha \le 1.0$	$10 \le p \le 1{,}000$ atm

Table 2. Typical Expansion Coefficient Values for Nitrides

Metal	Nitride	Z
Ti	TiN	1.0566
Zr	ZrN	1.0318
Hf	HfN	1.0145
Nb	NbN	1.1150
Ta	TaN	1.2620

Effect of pressure

As has been shown in previous studies, pressure of the gaseous reactant is very critical in filtration combustion. Here, cases pertaining to front propagation at low and high pressures are discussed.

Front propagation at high pressures is shown in Figures 4 and 5. Figure 4 shows time progression contour plots of temperature and conversion. In Figure 5 typical perspective plots for temperature, conversion, density and pressure are shown. The velocity vector plot for gas flow is shown in Figure 6. The pressure is high enough that $\alpha \simeq 1$. Ignition is achieved by heating the upper part of the solid material to the adiabatic temperature of the reaction, and maintained at that value for a certain period of time ($\bar{t} = t^H$). Given the high pressure of operation, there is uniform quantity of oxidizer available inside the system across the depth, thus the front becoming almost planar (Figure 4). However, there is a hot spot formed. This hot spot is a corrugation in the front produced due to the inequality between the rate at which heat is produced and the heat is diffused away. The corrugation protrudes into the cold region ahead of the front and uses up the solid reactant in that region and also draws in the gaseous reactant ahead of the front (see the vector plot). This

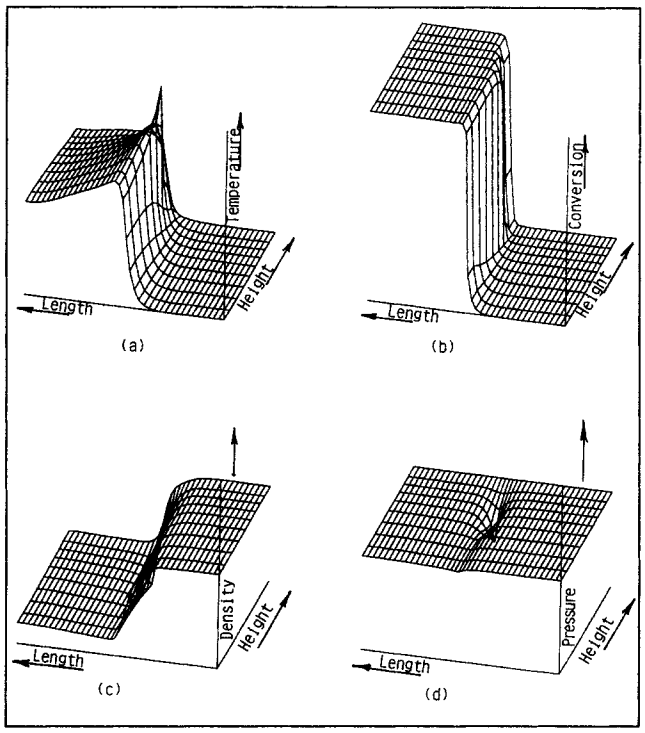

Figure 5. Three-dimensional perspective view of system parameters under high pressures.

$L_y = 5.0$, $L_x = 20.0$, $\alpha = 1.0$, $\beta = 0.08$, $\gamma = 0.05$, $\bar{t} = 16.0$: a. temperature, b. conversion, c. density, and d. pressure.

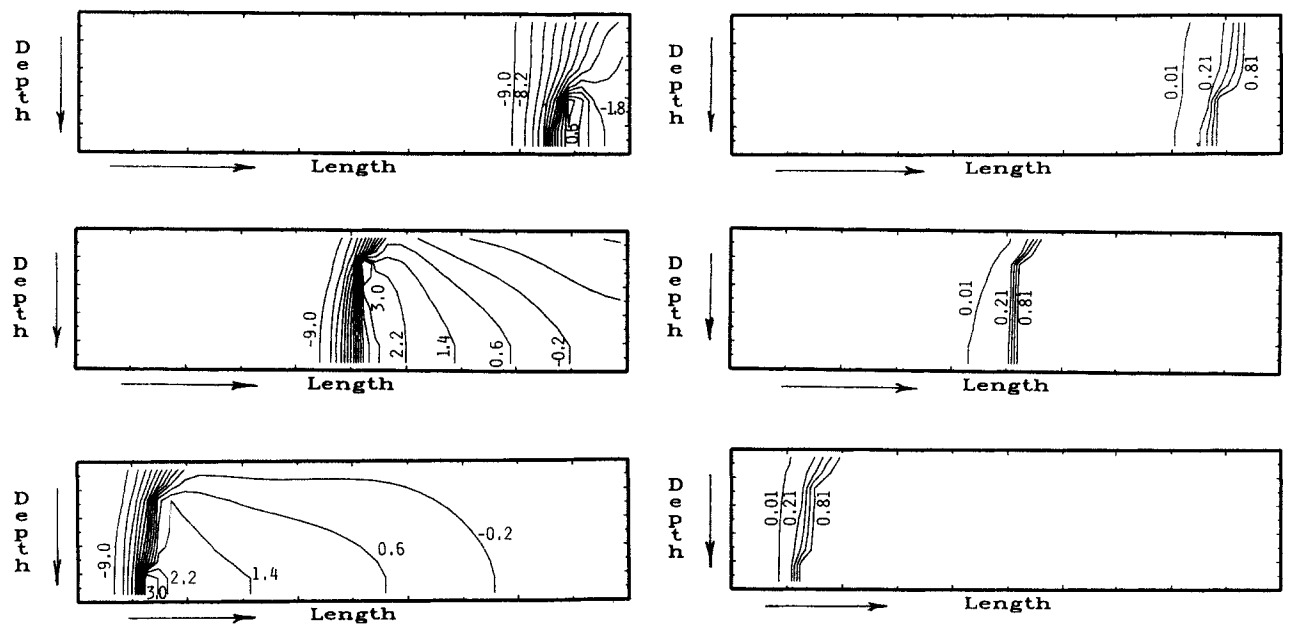

a. Temperature contours ranging from $\theta = -9.0$ to $\theta = 3.0$ in steps of 0.6

b. Conversion contours ranging from $\eta = 0.01$ to $\eta = 0.81$ in steps of 0.2

Figure 4. Reaction front propagation at high pressures.

$L_y = 5.0$, $L_x = 20.0$, $\alpha = 1.0$, $\beta = 0.08$, $\gamma = 0.05$. Increasing time from top to bottom $\bar{t} = 6, 16, 26$.

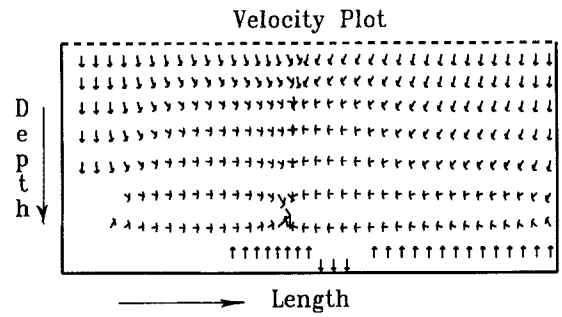

Figure 6. Gas velocity vector plot at high pressure.
$L_y = 5.0, L_x = 20.0, \alpha = 1.0, \beta = 0.08, \gamma = 0.05, \bar{t} = 16.0.$

causes the temperature to rise sharply in that region. While the hot spot dies eventually due to the depletion of solid reactant in that region, a new hot spot is formed elsewhere. Thus, this cycle is repeated, which makes hot spots oscillate between the top and the bottom as the front travels forward along the length. Since sufficient oxidizer is presented in the reactor at any time, the conversion is essentially complete. The rate of front propagation is controlled by the kinetics of the reaction; and the transport of gas due to filtration is not a limiting factor.

At significantly lower pressures ($\alpha = 0.01$) the propagation phenomena are markedly different. The amount of gas available at the bottom layer is only a fraction of the required stoichiometric quantity. In order for the reaction to be complete, the gaseous reactant needs to be transported by the process of filtration through the porous solid. In this case, the filtration resistance is the controlling factor in the reaction front propagation. There is an unequal supply of oxidizer between the upper and lower layer due to the longer filtration path length to the bottom of the reactor. As a result, the front propagation is skewed traveling ahead in the longitudinal direction at the top layer compared to that at the bottom. The conversion is complete at the top, while the inner layers are only partially reacted. As time progresses, however, the flow of oxidizer continues to the inner layers and the conversion progressively increases in that region. This sequence of events is shown in Figure 7. The perspective plots for the system parameters are shown in Figure 8. The gas velocity vector plot is shown in Figure 9. The gaseous oxidizer to the inner layers is fed not only by a transverse flow from layers immediately above them, but also from a longitudinal flow from regions far ahead of the front.

Effect of bed height

Given the unique nature of the cross flow configuration, the length of the powder bed does not affect the propagation once it is achieved. However, at very low pressures one of the critical factors affecting propagation of the reaction front is the bed height. The flow of gaseous oxidizer is driven by the pressure gradient between the external environment and the inner layers of the powder. At relatively low pressures (10–20 atm), corresponding to $0.005 < \alpha < 0.01$, the distance over which this change takes place has to be small enough to maintain sufficient gradient for driving the gas flow. The following cases at low pressures illustrate the importance of the bed height.

A set of simulations was carried out for $\alpha = 0.005$ to increase bed heights, keeping other parameters such as the length of the bed and the amount of initial energy input constant. Normal propagation as seen at low pressures is observed initially; however, after a certain height the front no longer propagates. At this stage, the rate at which the gas is transported to the front is not large enough to produce sufficient heat by reaction to balance out the heat losses due to conduction and convection from the front, and the heat lost to the surroundings, thus causing the front to extinguish. The low rates of gas flow are due to a decrease in driving force due to a much smaller pressure gradient. The pressure gradient is small due to the longer filtration path length and the lower external pressure. This has been illustrated in Figures 10 and 11. For a system with the bed height of $L_y = 2$, the combustion front propagates. However, when the bed height is increased to $L_y = 3.0$, the front extinguishes. In the latter case, only a small region near the point of initial ignition reacts (see Figure 11b). By increasing the pressure ($\alpha = 0.01$), the combustion front propagates (see

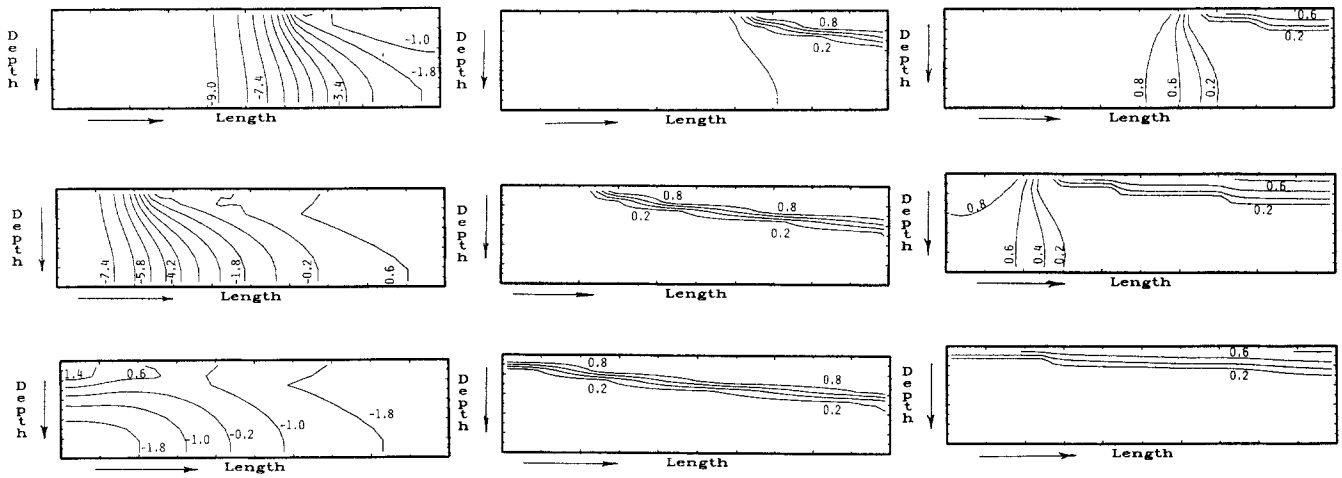

a. Temperature contours ranging from $\theta = -9.0$ to $\theta = 3.0$ in steps of 0.6

b. Conversion contours ranging from $\eta = 0.2$ to $\eta = 0.8$ in steps of 0.2

c. Pressure contours ranging from $\pi = 0.2$ to $\pi = 0.8$ in steps of 0.2

Figure 7. Reaction front propagation at low pressures.
$L_y = 5.0, L_x = 20.0, \alpha = 0.01, \beta = 0.08, \gamma = 0.05$. Increasing time from top to bottom $\bar{t} = 20, 40, 50$.

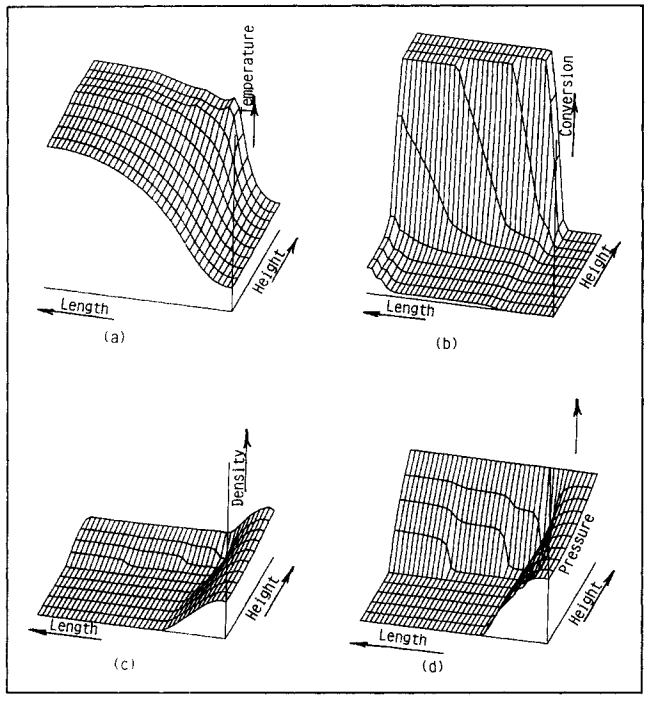

Figure 8. Three-dimensional perspective view of system parameters under low pressure.

$L_y = 5.0$, $L_x = 20.0$, $\alpha = 0.01$, $\beta = 0.08$, $\gamma = 0.05$, $\bar{t} = 40$: a. temperature, b. conversion, c. density, and d. pressure.

Figure 12). This observation indicates that there exists a certain depth of bed, above which the combustion front initially formed does not propagate.

Effect of porosity

An important factor in filtration combustion ignored in the past is the effect of variable porosity. An increase in porosity increases the permeability of the medium, which helps improve the accessibility of the gaseous oxidizer to the inner layers of solid. This is critical at very low pressures. However, thermal conductivity of the bed decreases as the porosity increases; as a result, the heat initially liberated at the point of ignition might not be easily dissipated. This might lead to extinction of the reaction front. To study these opposing effects, two numerical experiments with similar operating conditions, except for porosity and permeability of the medium, were performed. It was

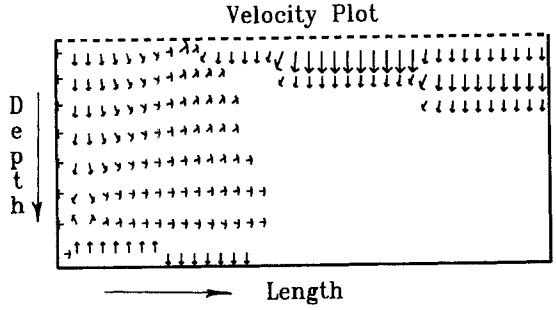

Figure 9. Gas velocity vector plot at low pressure.

$L_y = 5.0$, $L_x = 20.0$, $\alpha = 0.01$, $\beta = 0.1027$, $\gamma = 0.0625$, $\bar{t} = 40$.

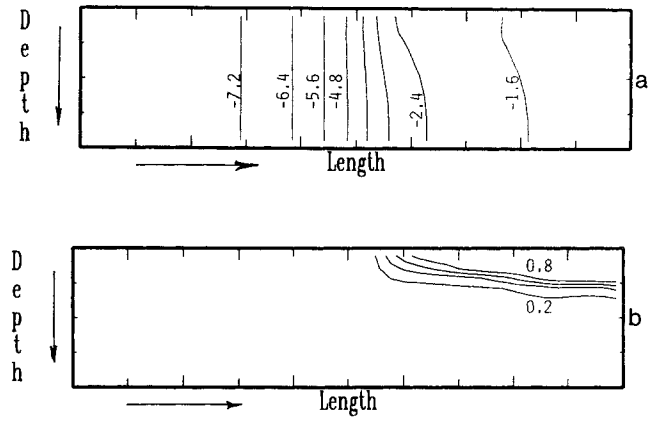

Figure 10. Effect of bed height: front propagation.

$L_y = 2.0$, $L_x = 20$, $\alpha = 0.005$, $\bar{t} = 30$: a. temperature contours varying from $\theta = -7.2$ to $\theta = -1.6$ in steps of 0.8; and b. conversion contours varying from $\eta = 0.8$ to $\eta = 0.2$ in steps of 0.2.

assumed that the change of porosity is due only to the expansion of the solid medium with reaction.

For the first case, the porosity was taken to be $\epsilon = 0.4$ and the permeability was taken to be $\omega = 35$. The heat was applied for the system for five dimensionless time units. The conversion and temperature profile at $\bar{t} = 40$ are shown in Figure 13, as well as the contours of the permeability. Due to the rapid conversion at the point of ignition, the porosity drops rapidly and so does the permeability of the medium. As a result, the access of gas is severely restricted and the front propagation stops due to insufficient gas at the front. The thermal conductivity is high, and all the heat is quickly dissipated to the rest of the system. The value of Z is taken to be 1.2, which is a reasonable value for certain transition metal-nitrogen systems (see Table 2).

The conditions for the second case are the same except that the porosity is now taken to be much higher ($\epsilon = 0.7$) leading to a permeability value of $\omega = 330$ (see Eq. 29). The profiles at time $\bar{t} = 11$ are shown in Figure 14. Unlike the previous case, despite the permeability drop, it does not drop significantly to

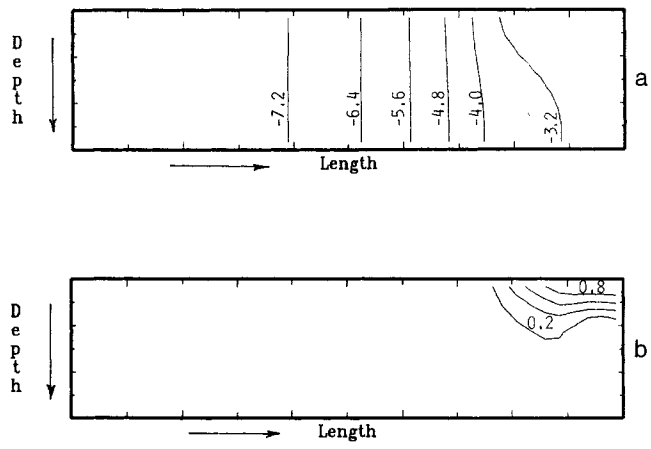

Figure 11. Effect of bed height: front extinction.

$L_y = 3.0$, $L_x = 20$, $\alpha = 0.005$, $\bar{t} = 30$: a. temperature contours varying from $\theta = -7.2$ to $\theta = -3.2$ in steps of 0.8; and b. conversion contours varying from $\eta = 0.8$ to $\eta = 0.2$ in steps of 0.2.

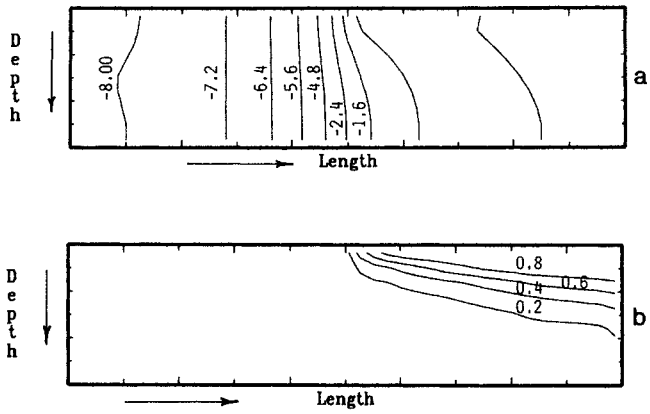

Figure 12. Effect of bed height: front propagation.

$L_y = 3.0$, $L_x = 20$, $\alpha = 0.01$, $\bar{t} = 30$: a. temperature contours varying from $\theta = -8.0$ to $\theta = -1.6$ in steps of 0.8; and b. conversion contours varying from $\eta = 0.8$ to $\eta = 0.2$ in steps of 0.2.

restrict the flow of gas to the inner layers. This is due to two reasons: its permeability has a higher value than the previous case; and because the solid is a smaller fraction of the whole medium, its conversion to products does not alter the porosity significantly. The system, in this case, propagates and eventually would completely convert the solid to products.

Comparison with experimental observation

To test the model, a set of simulations was performed using kinetic parameters obtained experimentally (Agrafiotis et al., 1990) for the system titanium and nitrogen. Activation energy

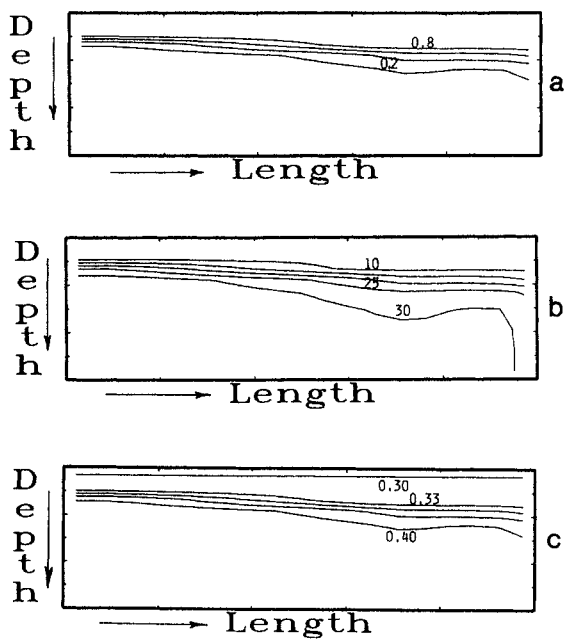

Figure 13. Effect of initial porosity: incomplete conversion for low initial porosity.

$\epsilon = 0.4$, $Z = 1.2$, $\omega = 35.0$, $L_x = 10.$, $L_y = 3.0$, $\alpha = 0.01$, $\bar{t} = 40$: a. conversion contours varying from $\eta = 0.2$ to $\eta = 0.8$ in steps of 0.2; b. dimensionless permeability (ω) contours varying from $\omega = 30.0$ to $\omega = 10$ in steps of 5; and c. porosity of the bed varying from $\epsilon = 0.28$ to $\epsilon = 0.40$ in steps of 0.024.

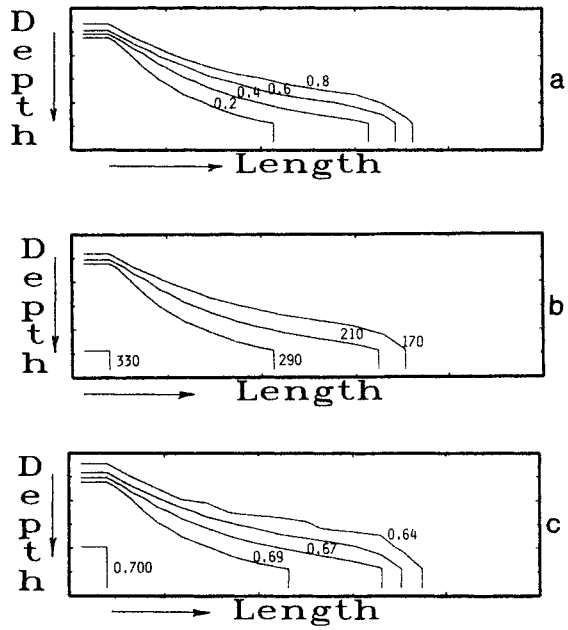

Figure 14. Effect of initial porosity: higher conversion for higher initial porosity.

$\epsilon = 0.7$, $Z = 1.2$, $\omega = 330.0$, $L_x = 10.0$, $L_y = 3.0$, $\alpha = 0.01$, $\bar{t} = 11$: a. conversion contours varying from $\eta = 0.2$ to $\eta = 0.8$ in steps of 0.2; b. dimensionless permeability (ω) contours varying from $\omega = 170.0$ to $\omega = 330.0$ in steps of 40; and c. porosity of the bed varying from $\epsilon = 0.644$ to $\epsilon = 0.70$ in steps of 0.014.

for the system was evaluated from nonisothermal measurements of reaction front velocity and combustion temperature for different degrees of solid-phase dilution. The heat of reaction and the adiabatic temperature rise were calculated using physical constants obtained from the *Chemkin Thermodynamic Database* (Kee et al., 1987). The measured activation energy, calculated adiabatic temperature rise, and thermo-physical properties describing the titanium-nitrogen system are listed in Table 3. Values of dimensionless parameters are given in Table 4.

Using these parameters, full two-dimensional simulations of combustion front propagation were performed. The calculated velocity of the combustion front was constant, and no oscillations were observed for all examined degrees of dilution. The

Table 3. Physical Parameters for the Simulation of Combustion Synthesis of Titanium Nitride

Parameter	Value
Heat of reaction	112.80 kJ · mol^{-1}
Activation energy	269.547 kJ · mol^{-1}
Sp. heat of nitrogen	1,200.00 J · mol^{-1} · K^{-1}
Sp. heat of titanium	648.90 J · mol^{-1} · K^{-1}
Sp. heat of titanium nitride	916.44 J · mol^{-1} · K^{-1}
Order with respect to gas	1
Order with respect to solid	1
Permeability	3.5×10^{-7} m^3 · s^{-1} · kg^{-1}
Initial porosity	60.00 %
Thermal conductivity of bed	10 W · m^{-1} · K^{-1}
Pressure	5 MPa
Adiabatic temperature	3,061-3,751 K
Convective heat transfer coeff.	187.5 W · m^{-2} · K
Radiative heat transfer coeff.	362.5 W · m^{-2} · K

Table 4. Dimensionless Coefficients Used in the Simulation of Combustion Synthesis of Titanium Nitride

Parameter	Value
α	0.065
β	0.094-0.1157
γ	0.0796-0.1196
θ_o	-8.156 to -5.42
θ^H	0.0
δ_1	0.5455
δ_2	1.8249
ω	300

thermal conductivity of the loose titanium-titanium nitride powder mixture, as used in the simulations, was measured from steady-state measurements of temperature profiles in a procedure similar to Yagi et al. (1960). The permeability measurements were made in the laboratory using the technique discussed by Kaye (1967).

The experiments were performed in a stainless steel autoclave, capable of withstanding 400 atm. The vessel was equipped with ports for thermocouples, a camera, a pressure transducer, and leadthroughs for electrodes. The sample was placed in a flat-bottomed rectangular container in the form of loose powder and ignited with a chemical igniter, similar to the configuration shown in Figure 2. The front propagation for the Ti-N_2 system at elevated pressures was monitored using a video camera attached to the high-pressure reactor and the images recorded. The recordings clearly indicate the presence of constant velocity propagating front. The front velocity was evaluated from these observations. These measured velocities were compared with those calculated under identical conditions, and reasonable quantitative agreement was achieved (see Table 5).

Conclusions

While the filtration combustion process has received considerable attention in the past few years, there has been a lack of detailed numerical study in this area. For the first time, an effort has been made to solve an unsteady-state, two-dimensional model for the process numerically. Use of fast vector computers and novel adaptive grid schemes have made this feasible. It is hoped that this study will aid in the detailed numerical modeling of the filtration combustion and SHS technology in general. Numerical modeling can help understand and exploit the SHS process toward production of many important high-temperature materials.

Based on the numerical simulations, the following conclusions can be drawn:

- The system pressure strongly governs the front propagation phenomena. At low pressures, the front is often skewed traveling ahead in the upper layers compared to the inner layers, thus causing potential incomplete conversion in some cases. At high pressures, sufficient gas is available in the system so that the conversion of the solid reactant is complete. However, excessively high temperatures may be produced in such cases and lead to melting or sintering of solid, which is not desirable.
- At low pressures, the height of solid layer is critical. If the height is too large then the pressure gradient to drive the gas toward the inner layers is too small, as a result the front extinguishes. It has been found that there exists a certain depth of bed for a particular pressure of operation, which if exceeded causes a combustion front, initially formed, to extinguish.
- Another critical factor is the porosity of the solid. When the reaction is accompanied by an increase in volume of the solid, conversion of the solid reactant leads to decrease in porosity. Since the permeability of the system is a strong function of the porosity of the system, the gas flow to the inner layers is severely restricted. This might cause only the upper layers of the system to react leaving unconverted solid reactant at the bottom. To avoid this situation, the initial bed porosity should be high to make sure that there is sufficient access for the gas to the inner layers of solid reactant.
- Preliminary comparisons with experimental observations have shown that the model gives good order of magnitude predictions.

The model, even though reasonably detailed, is still quite simplified in certain aspects and should be used only as a qualitative tool for predicting front phenomena. For low reactor widths, the third dimension and the wall effects cannot be neglected either. When the dilution of the solid phase is low, significant melting of the solid phase may occur, given the higher reaction temperatures. These effects need to be taken into account both in the heat balance and in the relations for change of porosity. The observations in this study, which show a better agreement of the simulation results with the experimental observations a higher solid-phase dilutions, add weight to this argument.

Table 5. Comparison of Experimental and Theoretical Velocities

Dilution Ti-TiN wt. %	T_* K	V (Experiment) $10^3 \times$ m/s	V (Simulation) $10^3 \times$ m/s
50-50	3,751	5.6	3.70
40-60	3,310	2.5	2.7
35-65	3,061	1.3	1.27

Acknowledgment

This work was supported in part by NSF Grant CTS 8915787. The computations were performed using a CRAY X-MP/48 at the National Center for Supercomputing Applications at the University of Illinois at Urbana-Champaign, through a NSF grant (CBT 890018N) for supercomputing resources. The authors would like to thank Jan Degreve for his help in developing the computer code and Chris Agrafiotis for sharing his experimental results, as well as their constant input in several discussions.

Notation

c = specific heat, $J \cdot K^{-1} \cdot kg^{-1}$
E = activation energy, $J \cdot mol^{-1}$
$(-\Delta H)$ = heat of reaction, $J \cdot kg^{-1}$
h_c = convective heat transfer coefficient, $W \cdot m^{-2} \cdot s^{-1}$
h_r = radiative heat transfer coefficient, $W \cdot m^{-2} \cdot s^{-1}$
$\hat{H}$ = enthalpy per unit volume, $J \cdot m^{-3}$
k = filtration coefficient of the system, $m^3 \cdot s \cdot kg^{-1}$
k_o = frequency factor
L_x = bed length, m
L_y = bed height, m
M = molecular weight
n = order of reaction with respect to solid,
p = pressure, $N \cdot m^{-2}$
R = universal gas constant, $8.314\ J \cdot mol^{-1} \cdot K^{-1}$
t = time, s
T = temperature, K

$\hat{U}$ = internal energy per unit volume, $J \cdot m^{-3}$
v = velocity of gas, $m \cdot s^{-1}$
W = consumption rate of solid, $kg \cdot m^{-3} \cdot s^{-1}$
x = length coordinate, m
y = height coordinate, m
Z = expansion coefficient for solid reactant

Greek letters

α = measure of stoichiometric gas amount in Void
β = dimensionless activation energy
γ = dimensionless heat of reaction
δ = ratio of specific heats
ϵ = void fraction
λ = effective thermal conductivity, $W \cdot m^{-1} \cdot K^{-1}$
μ = stoichiometric coefficient
ν = order of reaction with respect to gas
η = partial conversion of solid
ω = dimensionless permeability coefficient
π = dimensionless pressure
ρ = density, $kg \cdot m^{-3}$
ρ_P = bulk density of solid product, $kg \cdot m^{-3}$
ρ_R = bulk density of solid reactant, $kg \cdot m^{-3}$
θ = dimensionless temperature

Subscripts and superscripts

1 = gas to solid reactant ratio
2 = product to solid reactant ratio
g = gas
H = hot boundary
o = initial condition
P = solid product
R = solid reactant
s = solid
$-$ = dimensionless
$*$ = reference value

Literature Cited

Agrafiotis, C., J. A. Puszynski, and V. Hlavacek, "Experimental Study of the Synthesis of Titanium and Tantalum Nitride in the Self-Propagating Regime," *Comb. Sci. Tech.*, in press (1990).

Aldushin, A. P., A. G. Merzhanov, and B. I. Khaikin, "Conditions for the Layered Filtration Combustion of Porous Metals," *Dokl. Akad. Nauk SSSR*, **215,** 612 (1974).

Aldushin, A. P., A. G. Merzhanov, and B. S. Seplyarskii, "Theory of Filtration Combustion of Metals," *Fiz. Gor. Vzryva*, **12,** 323 (1976).

Aldushin, A. P., B. S. Seplyarskii, and K. G. Shkadinskii, "Theory of Filtration Combustion," *Fiz. Gor. Vzryva*, **16,** 36 (1980).

Aldushin, A. P., and S. G. Kasparyan, "Stability of Stationary Filtration Combustion Waves," *Fiz Gor. Vzryva*, **17,** 37 (1981).

Bird, R. B., W. Stewart, and E. Lightfoot. *Transport Phenomena*, Wiley, New York, Ch. 10, p. 313 (1960).

Carman, P. C., "Fundamental Principles of Industrial Filtration," *Trans. Inst. Chem. Eng. London*, **16,** 168 (1938).

Dandekar, H. W., "Raster Graphics and Animation," *Interface*, State Univ. of New York, Buffalo, **20,** 3 (1989).

Dandekar, H. W., J. A. Puszynski, J. Degreve, and V. Hlavacek, "Reaction Front Propagation Characteristics in Non-Catalytic Exothermic Gas-Solid Systems," *Chem. Eng. Comm.*, **92,** 199 (1990).

Degreve, J., "Use of Adaptive Meshes in Simulation of Combustion Systems," PhD Diss., State Univ. of New York, Buffalo (1990).

Degreve, J., P. Dimitriou, J. Puszynski, V. Hlavacek, S. Valone, and R. Behrens, "Numerical Resolution of Front Phenomena by Regridding Techniques," *ACS Symp. Ser.*, **353,** 376 (1987).

Kaye, B. H., "Permeability Techniques for Characterizing Fine Powders," *Powder Tech.*, **1,** 11 (1967).

Kee, R. J., F. M. Rupley, and J. A. Miller, "The Chemkin Thermodynamic Database," *Sandia Report*, SAND87-8215. UC-4, Sandia National Laboratories, Albuquerque, NM (1987).

Kumar, S., "Self-Propagating High Temperature Synthesis of Ceramic Materials," PhD Diss., State Univ. of New York, Buffalo (1988).

Kumar, S., C. C. Agrafiotis, J. A. Puszynski, and V. Hlavacek, "Heat Transfer Characteristics in Combustion Synthesis of Ceramics," *AIChE Symp. Ser.*, **263,** 50 (1988).

Merzhanov, A. G., A. K. Filonenko, and I. P. Borovinskaya "New Phenomena in Combustion of Condensed Systems," *Dokl. Akad. Nauk SSSR*, **208,** 892 (1973).

Merzhanov, A. D., and I. P. Borovinskaya, "A New Class of Combustion Processes," *Comb. Sci. Tech.*, **10,** 195 (1975).

Munir, Z. A., "Synthesis of High Temperature Materials by Self-Propagating Combustion Methods," *Cer. Bull.*, **67,** 342 (1988).

Munir, Z. A., and J. B. Holt, "The Combustion Synthesis of Refractory Nitrides: 1. Theoretical Analysis," *J. Mat. Sci.*, **22,** 710 (1987).

Roache, P. J., *Computational Fluid Dynamics*, p. 65, Hermosa Publishers, Albuquerque, NM (1972).

Sukhov, G. S., and L. P. Yarin, "Two-Dimensional Instability of the Combustion of Porous Substances in Gaseous Oxidizer," *Fiz. Gor. i. Vzryva*, **16,** 34 (1980).

Szekely, J., J. W. Evans, and H. Y. Sohn, *Gas-Solid Reactions*, Academic Press, New York (1976).

Yagi, S., D. Kunni, and N. Wakao, "Studies on Axial Thermal Conductivities in Packed Beds," *AIChE J.*, **6,** 543 (1960).

Manuscript received Jan. 31, 1990, and revision received Aug. 23, 1990.

See NAPS document no. 04805 for 4 pages of supplementary material. Order from NAPS c/o Microfiche Publications, P.O. Box 3513, Grand Central Station, New York, NY 10163. Remit in advance in U.S. funds only $7.75 for photocopies or $4.00 for microfiche. Outside the U.S. and Canada, add postage of $4.50 for the first 20 pages and $1.00 for each of 10 pages of material thereafter, $1.50 for microfiche postage.